Chemical Papers
https://doi.org/10.1007/s11696-022-02222-z

ORIGINAL PAPER

Melatonin photoreactivity: phosphorescence formation and quenching processes

Kristján Einar Guðmundsson[1,3] · Guðrún Marteinsdóttir[1,2] · Kristberg Kristbergsson[1,2] · Ágúst Kvaran[3]

Received: 14 February 2022 / Accepted: 9 April 2022
© The Author(s) 2022

Abstract

Studies of melatonin photoreactivity in water solutions: An effect of an external heavy atom I^- on UV/Vis absorption, fluorescence and phosphorescence spectra is explored. The data allowed determination of relevant energetics for the system. The heavy atom effect (HAE) of I^- on melatonin is clearly found to induce an intersystem crossing from the lowest energy singlet state to the lowest energy triplet state (T_1) by a state mixing. Lifetime for the first excited triplet states of melatonin in association with I^- and quenching rates for halomethanes (CH_2X_2, CHX_3, CY_4, X = Cl, Br, Y = Cl) are determined from Time-Correlated Single-Photon Counting decay curves for the phosphorescence. Dramatic alterations in quenching rate constants with quenchers as $CH_2X_2 < CHX_3 < CX_4$ and Cl < Br are attributed to energy transfer from an $I^{-}\cdots Me^{*}(T_1)$ complex to low-lying electronic states of the halomethanes followed by dissociation to form R and X fragments. Relevance of the melatonin photoreactivity to photosensitizer properties in organic media is discussed.

Graphical abstract

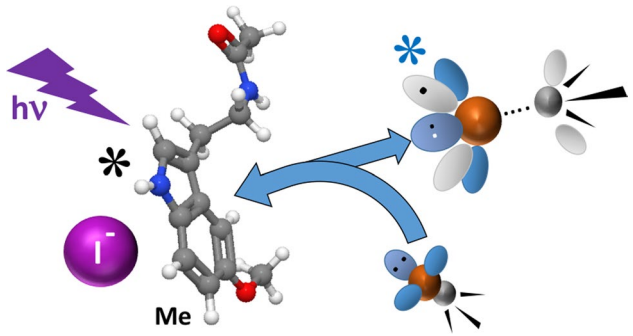

Keywords Phosphorescence · Quenching · Melatonin · Intersystem crossing · Photosensitizer · TCSPC

✉ Ágúst Kvaran
agust@hi.is

Kristján Einar Guðmundsson
keg9@hi.is

Guðrún Marteinsdóttir
runam@hi.is

Kristberg Kristbergsson
kk@hi.is

[1] Faculty of Food Science and Nutrition, University of Iceland, Sæmundargata 2, 101 Reykjavík, Iceland

[2] Taramar Ehf, Miðnestorg 3, 245 Sandgerði, Iceland

[3] Science Institute, University of Iceland, Dunhagi 3, 107 Reykjavík, Iceland

Introduction

Molecules exhibiting luminescence in the form of fluorescence and phosphorescence have become a popular area of research in studies relating to protein folding (Mersol, Gershenson et al. 1992; Mersol et al. 1993; Gershenson et al. 2000; Kowalska-Baron et al. 2015) as well as in the development of photosensitizers for various purposes (Kuijt et al. 2003; Alvarez-Lorenzo et al. 2009; Jin and Zheng 2011; Lajunen et al. 2016; Salem et al. 2019). Quenching processes of the luminescence are important aspects of these studies (Kim et al. 1990; Gershenson et al. 2000; Jayaraj et al. 2010;

Published online: 13 May 2022

Massiot et al. 2017). One such molecule is indole, along with its derivatives tryptophan, melatonin and NATA (N-Acetyl-L-tryptophanamide). The structure of indole is that of a benzene ring fused with a heterocyclic pyrrole ring from where the aforementioned luminescence arises. This family of molecules is known to absorb strongly in the 290 nm region due to nonbonding to π antibonding (n-π^*) orbital transitions followed by fluorescence (Strambini and Gonnelli 1995; Strambini et al. 2004; Kowalska-Baron et al. 2012; Kowalska-Baron et al. 2013). Under certain circumstances, a population of the first excited triplet state (T_1) via inter-system crossing can occur (Strambini et al. 2004; Amjadi et al. 2006; Kowalska-Baron et al. 2012, 2013). Relaxation of T_1 to form the ground state (S_0) either occurs via radiationless deactivation or by emission of photons (phosphorescence). The lifetime of the triplet state of indole has been measured by various groups using both sensitive photon-counting methods and flash photolysis, which has yielded considerable disagreement regarding its value (Bent and Hayon 1975; Strambini et al. 2004; Kowalska-Baron et al. 2012, 2013). The original lifetime of 12 µs, published in 1975 by Bent and Heyon, who used flash photolysis, has since been improved upon by Strambini et al. which in 1995 reported it to be 1.2 ms (1200 µs) (Bent and Hayon 1975; Strambini and Gonnelli 1995). This long lifetime was questioned by Fischer et al. in 2001 (Fischer et al. 2002), who claimed it to stem from a photochemistry by-product stabilized by impurities. In this paper, Fischer et al. reported a lifetime of 40 µs using the photon counting technique (Fischer et al. 2002). The long lifetime was reiterated in 2004 in reanalysis by Strambini et al. who obtain a lifetime of 5 ms by taking special care of impurities (Strambini et al. 2004). Further investigation of the lifetime of indole was made by Kowalska-Baron et al. by the application of the heavy atom effect (HAE) as a means to reduce a possible alternate pathways from the S_1 state. By using potassium iodide to enhance spin–orbit (SO) coupling, Kowalska-Baron et al. reported a lifetime of 60 µs by the use of the photon-counting technique (Kowalska-Baron et al. 2012). The difference in T_1 lifetimes for indole and its derivatives has been found to be minor according to Strambini (1.2, 1.16 and 1.2 ms reported in 1995 for indole, tryptophan and NATA (Strambini and Gonnelli 1995), respectively, and 5.1 and 5.0 ms for indole and NATA in 2004, respectively (Strambini et al. 2004)). A more dramatic variance in the lifetime of T_1 was, however, observed in 2012 by Kowalska-Baron et al. (110.6, 80.5 and 68.3 µs for indole, tryptophan and NATA, respectively), which hints at the influence of the functional groups of NATA and tryptophan (Kowalska-Baron et al. 2012). This influence was further probed in 2013, where Kowalska-Baron et al. reported T_1 lifetimes of 912 and 56 µs for indoles carboxylated in positions 2 and 5, respectively.

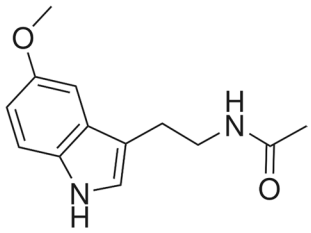

Scheme 1 Melatonin ($C_{13}H_{16}N_2O_2$)

Structurally, melatonin (N-acetyl-5-methoxytryptamine) is dissimilar to indole by the two functional groups, acetamide and methoxy attached to positions 2 and 5, respectively, of the aromatic indole unit (Scheme 1). Less has been published regarding the chromophoric nature of melatonin than that of indole or its other derivatives tryptophan and NATA. The body of research has been focused on its application as a stabilizer of micelles or cyclodextrins in aqueous media where its luminescence is subject to various quenching processes depending on the environment (de Lima et al. 2010; Drolle et al. 2013; Reiter et al. 2014; Bolmatov et al. 2019). The favored application of melatonin as a micelle stabilizer over other popular antioxidants arises from two features which make it optimal for this purpose, i.e., its ability to form stable oxidized products that furthermore act as antioxidants and its ability to interact with, and stabilize the phospholipid membrane (Goswami and Haldar 2015; Bolmatov et al. 2019; Zhang et al. 2021). The fluorescent lifetime of melatonin has been reported to be 5.9 ns in aqueous solution of pH = 7 (Rath et al. 1999). Amjadi et al. reported the triplet state lifetime of melatonin to be 107 µs by the application of the photon counting technique, which is close to the value of 110.6 µs for indole reported by Kowalska-Baron et al. (Amjadi et al. 2006; Kowalska-Baron et al. 2012). Amjadi et al. studied the effect of the common heavy atom effect (HAE) inducer I^- and pH on the phosphorescence of melatonin in solutions. They used sodium sulfite, rather than a degassing/pumping deoxygenation system, which proved to be very efficient oxygen scavenger (Amjadi et al. 2006). In 1999, Rath et al. reported rate constants for quenching of the fluorescence of melatonin due to the $S_1 \rightarrow S_0$ transition by organic halides to be of the same order of magnitude as that of molecular oxygen ($\approx 10^{10} M^{-1} s^{-1}$) (Rath et al. 1999).

The above-mentioned chromophores are subject to quenching by solution impurities and molecular oxygen depending on the molecule movements/temperature. Luminescence due to transitions from the T_1 state is rarely observed at room temperature. Consequently, many of preceding phosphorescence studies have been conducted at cryogenic temperatures for glass states of solutions to limit radiationless decay processes (Aaron et al. 1974;

Kotel'nikova et al. 1982; Imakubo 1985; Li and Galley 1989; Krasnovsky et al. 1999). At higher and ambient temperatures, this obstacle has been overcome by the use of various methods for increasing the probability of the luminous pathway. This includes to increase the rate of $S_1 \rightarrow T_1$ intersystem crossing by enhancement of spin–orbit (SO) coupling as well as methods of molecular oxygen exclusion. Increased phosphorescence has been observed for tryptophan residues in large proteins compared to that of free tryptophan. This is due to the fact that the hydrophobic areas are buried in the interior of the large proteins, which restricts the chromophore movement and quenching processes. Advantage has been taken of this scenario by the use of host–guest systems such as encapsulation by cyclodextrins, liposomes and closed nano-containers (Jayaraj et al. 2010; Montes-Navajas and Garcia 2010; Easley et al. 2018).

The major low-energy external luminescence (phosphorescence and fluorescence) quenchings for aromatic compounds are due to (i) heavy atom effects and (ii) energy transfer. (i) The external heavy atom (EHA) effect is associated with an increasing spin–orbit coupling between the excited singlet and triplet states of the aromatic compound in the presence of an external heavy atom in relevant complexes (Giachino and Kearns 1970; Braslavsky and Houk 2003; Minaev 2004). The interaction with the heavy atom enhances transfer from singlet excited states to triplet excited states (i.e., $S_1 \rightarrow T_1$ transition) to reduce the fluorescence due to the $S_1 \rightarrow S_0$ transition and to increase the corresponding phosphorescence due to the $T_1 \rightarrow S_0$ transition. The effect of an increasing phosphorescence can also be explained by an intensity borrowing due to enhanced mixing of the triplet states (T_1) with the singlet state (S_1), to cause an increasing singlet character, induced by the heavy atom interaction with the molecule (Minaev 2004). The effect is found to increase largely with atom (e.g., $Ne \sim Ar < Kr << Xe$; see reference (Minaev 2004)) and ion (e.g., $F^- \sim Cl^- < Br^- < I^-$; see reference (White and Seybold 1977)) sizes and to decrease largely with the distance between the heavy atom and the emitting molecule (Najbar et al. 1978). (ii) Energy transfer involves radiationless transition of the excess energy of the excited state molecule to a quenching molecule. The major energy transfer is in the form of electronic energy exchange. Thus, the well-known quenching of a molecule phosphorescence by oxygen typically involves radiationless transition from a triplet state to a ground singlet state within the molecule as the oxygen molecule is excited from its triplet ground state to a singlet excited state (Egorov et al. 1999; Lepeshkevich et al. 2014; Di Mascio et al. 2019; Qin et al. 2019). Any energy mismatch of the electronic energies for the two species will result in excess kinetic energies in the form of vibrational, rotational and/or translational energies.

Since emitting states in fluorescence (S_1) and phosphorescence (T_1) typically correspond to the lowest energy excited electronic states of the molecules, an efficient quenching involving an electronic energy transfer requires still lower electronic energies for the quenchers. The halomethanes are rich in low-energy singlet and triplet valence states associated with excitation of electrons in nonbonding halogen orbitals (n) to antibonding σ^* orbitals (RCl (Eden et al. 2007); RBr (Causley and Russell 1975; Van Veen et al. 1985; Escure et al. 2009)). The density and degeneracy of states increase with number of halogens in the molecules. Furthermore, judging from the appearance of the corresponding absorption spectra (Keller-Rudek et al. 2013) the excited state energies lower as the number of halogen atoms increases. The corresponding potential energy curves as a function of the carbon-halogen (C–X) bond energy for the methyl-monohalides are found to be repulsive, which forms the basis for a halogen atom formation by photodissociation (CH_3Cl (Granucci et al. 2010); CH_3Cl and CH_3I (Ajitha et al. 2004; Eden et al. 2007); CH_3Br (Van Veen et al. 1985; Blanchet et al. 2009; Escure et al. 2009); CH_3Br (Van Veen et al. 1985; Hafliðason et al. 2018, 2019); CH_3I (Matthíasson et al. 2020)).

In this paper, we present energetic information of the indole derivative, melatonin (Scheme 1), relevant to its photophysics dynamics, based on absorption, fluorescence and phosphorescence spectra as a function of various solvent condition parameters. Phosphorescence is strongly induced by a heavy atom effect. Quenching of the phosphorescence, by number of chlorine and bromine containing halomethanes, was determined and found to be consistent with an energy transfer to low-lying electronic states, which will be followed by a bond dissociation of the quenching molecules.

Experimental and analysis methods

Absorption, fluorescence and phosphorescence spectra of melatonin in the presence of I^- as a heavy atom quencher (from KI(s)), oxygen scavenger (SO_3^{2-} from Na_2SO_3(s)/sodium sulfite) (see reference (Amjadi et al. 2006)) with or without halomethane quenchers in different concentrations in a buffer solution of pH = 8.8 were recorded. The fluorescence and phosphorescence spectra were obtained for 290 nm excitation. Time-resolved phosphorescence at 457 nm was recorded as a function of the halomethane quencher concentration to derive relevant phosphorescence lifetimes. Quenching rate constants were derived from corresponding Stern–Volmer plot analysis. More details are as follows (see also supporting material).

For absorption spectra, fresh solutions of melatonin (5.22×10^{-4} M) and potassium iodide (KI) (2.0 M) were prepared prior to dilution (typically 1.74×10^{-4} M (melatonin),

1.2 M and 0.4 M (KI)). Tris buffer of 0.5 M, pH 8.8 was used. The concentration for melatonin was chosen to keep the maximum absorbance of a solution without KI and quenchers at 290 nm of about 1. For luminescence spectra and relevant analysis, a stock solution of anhydrous sodium sulfite (0.1 M) was prepared monthly and kept refrigerated. A melatonin solution of 5.6×10^{-5} M was prepared and kept frozen until analysis. A fresh solution of potassium iodide (2.0 M) was prepared, and a Tris buffer of 5×10^{-2} M, pH 8.8 was used. Prior to the analysis, aliquots of the aforementioned solutions were diluted for final concentrations (typically 6.5×10^{-7} M (melatonin), 0.4 M and 1.2 M (KI) and 2×10^{-2} M (sodium sulfite), based on values given by Amjadi et al. (Amjadi et al. 2006). The lowest concentrations of the quenchers ($CHCl_3$, CH_2Cl_2, CCl_4, $CHBr_3$ and CH_2Br_2) were added followed by the Tris buffer to create a final volume of 3 mL. The concentrations of the quenchers were increased by its addition to the original solutions. 1.0-cm Hellman quartz cuvettes (Art. Nr. 110-10-40) (Hellma Analytics (Tustin, USA)) were used. The cuvettes with solutions were inverted before analysis to ensure homogeneity.

Absorbance spectra were recorded by the use of a Thermo Scientific Evolution 350 double-beam UV–Vis spectrophotometer (Thermo Fischer Scientific Inc. (Massachusetts, USA)). The spectra were recorded for a blank consisting of the Tris buffer in water. Steady-state fluorescence and phosphorescence spectra were recorded by the use of a Fluoromax-4P phosphorimeter equipped with a Xenon flash lamp (Horiba Ltd. (Kyoto, Japan)) and controlled by the use of the Fluorescence software (Horiba Ltd. (Kyoto, Japan)). All scans were made between 320 and 550 nm using the analytical parameters of the excitation set at 290 nm and slit width of 15 nm. Time-resolved phosphorescence analysis was performed by using the Fluoromax-4P phosphorimeter equipped with a Horiba FluoroHub (Horiba Ltd. (Kyoto, Japan)) time-correlated single-photon detector. Excitation was set at 290 nm with a slit width of 1 nm while the emission was recorded at 457 nm with slit width of 8 nm. The measurement range used was of 2.7 ms (2048 channels, each containing 1333.336 ns). The selected parameters were chosen to avoid "photon pile-up" effect (corresponding to $\alpha<2.0\%$).

Time-Correlated Single-Photon Counting (TCSPC) data points, which are directly proportional to the emission intensity for phosphorescence measurements, were exported from the DAS6 software (Horiba Ltd. (Kyoto, Japan)) versus channels and further processed by using the IGOR Pro software (Wavemetrics, Inc. (Oregon, USA)). The channel numbers were transferred to nanoseconds to obtain the data in the form of intensity (I) versus time (t) followed by a logarithmic transformation of the intensity ($\ln(I)$) to obtain the lifetime from slopes of linear plots of $\ln(I)$ versus t. Finally, quenching rate constants were derived from the reciprocal of the lifetime as a function of quencher concentrations (Stern–Volmer plots). See more details in next section under "Quenching by halomethanes" The data points used for each set of experiments were in the range of 150–350 points. A linear regression analysis was performed using the weight of the standard deviation of points.

Results and analysis

Spectra, energetics and intersystem crossing

Figure 1 shows absorption (a), fluorescence (b) and phosphorescence (c) spectra for melatonin in solutions of different concentrations of KI. Specification of other solution components is indicated in the figure caption. The luminescence spectra (Fig. 1b, c) are created by 290 nm excitation. The major characteristics of the spectra and spectra changes with KI concentration are as follows:

(a) (Fig. 1a) The absorption spectrum of melatonin in a solution without KI shows absorption due to the $S_1\leftarrow S_0$ transition in the spectral range of about 250–325 nm and due to transitions from S_0 to higher energy singlet states (S_n; $n=2,\ldots$) for wavelengths less than about 250 nm. No absorption is detected for wavelengths longer than about 325 nm. The major effect of adding and increasing the KI concentration is firstly that a broad absorption band peaking near 355 nm appears and increases and secondly that an additional absorption, apparently due to transitions to higher-order singlet states, appears in the spectral region of about 230–275 nm. Furthermore, the absorption due to the $S_1\leftarrow S_0$ transition appears to increase, but an enhanced contribution of spectra tails due to transitions to the higher-lying singlet states (S_n) in that region cannot be ruled out. The selected concentration of melatonin for this analysis was based on the retrieval of spectra with the 290 nm absorbance in the range of 0.9–1.0.

(b) (Fig. 1b) The fluorescence spectra created by a 290 nm excitation correspond to the $S_1\leftarrow S_0$ transition. The spectrum of melatonin in a solution without KI is bimodal in shape with peak maxima at about 327 nm and 395 nm. These reflect transitions from the lowest energy excited singlet state (S_1) to an energy range within the S_0 state for different vibrational modes and energy-dependent transition probabilities. As an increasing amount of KI is added, the fluorescence intensity is rapidly quenched and the spectral shape changes severely. Judging from the spectral shape changes („difference spectra"; see Fig. 1b), the decreasing intensity closely corresponds to the melatonin (without KI) fluorescence spectral structure, suggest-

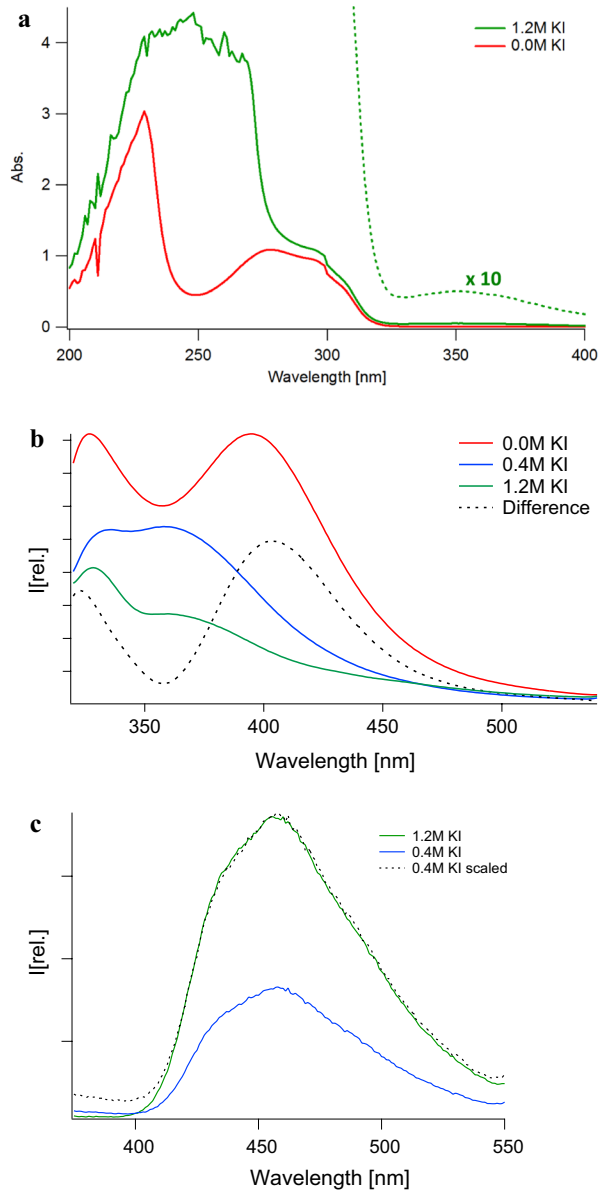

Fig. 1 **a** Absorption spectra of melatonin (1.74×10^{-4} M) buffered with Tris (0.5 M, pH 8.8) with and without heavy atom effect (HAE) inducer KI (see main text). An expansion of the spectrum (×10) with KI in the high wavelength region is inserted (dotted green curve). **b** Fluorescence spectra of melatonin (6.50×10^{-7} M) versus KI concentration for 290 nm excitation. Solution was buffered in Tris (0.5 M, pH 8.8) with sodium sulfite (2.0×10^{-3} M) as oxygen scavenger. Additionally presented is the difference between the spectra of 0.0 M and 0.4 M KI ("difference spectrum"). **c** Phosphorescence spectra of melatonin (6.50×10^{-7} M) versus KI concentration for 290 nm excitation. Solution was buffered in Tris (0.5 M, pH 8.8) with sodium sulfite (2.0×10^{-3} M) as an oxygen scavenger. Presented additionally is the 0.4 M KI spectrum scaled to the maximum of the 1.2 M KI spectrum

ing that it mainly involves quenching of the S_1 state. The concentrations of melatonin, potassium iodide and sodium sulfite used for these analyses were based on the study of Amjadi et al. (Amjadi et al. 2006).

(c) (Fig. 1c) No phosphorescence was detected for a solution of melatonin without KI for a 290 nm excitation. As an increasing amount of KI was added, phosphorescence appeared and increased in intensity. The spectral shape, however, did not change within experimental error for the KI concentration used. This corresponds to the $T_1 \rightarrow S_0$ transfer. A close correlation was found between the fluorescence intensity quenching (decrease) and the phosphorescence increase. Judging from these observations KI induces energy transfer/intersystem crossing from S_1 to T_1 prior to the forbidden $T_1 \rightarrow S_0$ radiative transition (phosphorescence).

The energetics and relevant energy transfer processes as shown in Fig. 2 can be derived from the spectral data. Upper and lower spectral limits of the absorption, fluorescence and phosphoresce spectra mentioned above allow estimates of state energy ranges as shown in Fig. 2 based on the following criteria.

(a) The excitation (290 nm) is assumed to correspond to a transition from the low-energy edge of the ground state S_0 to an intermediate region of the S_1 state (Fig. 2a, b).

(b) The emission corresponding to the fluorescence spectrum peaks for melatonin without KI (327 nm and 395 nm) is assumed to correspond to transitions from the low energy limit of the excited singlet state S_1 to an intermediate region of the S_0 state. The long wavelength edge of the fluorescence spectrum (ca. 450 + nm) is assumed to correspond approximately to a transition from the low energy limit of the excited singlet state S_1 to the high-energy edge of the S_0 state (Fig. 2a).

(c) The emission corresponding to the phosphorescence spectrum peak (457 nm) is assumed to correspond to transitions from the low energy limit of the excited triplet state T_1 to an intermediate region of the S_0 state (Fig. 2b).

Judging from this energetic analysis, the weak absorption band which peaks near 355 nm by adding KI (see above) corresponds to "the forbidden" transition from the ground state S_0 to the low energy range of the T_1 state below the S_1 state (Fig. 2b). This clearly indicates an external heavy atom effect of I^- on an enhanced transition probability/intensity borrowing due to the $S_1 \leftrightarrow T_1$ state mixing/coupling.

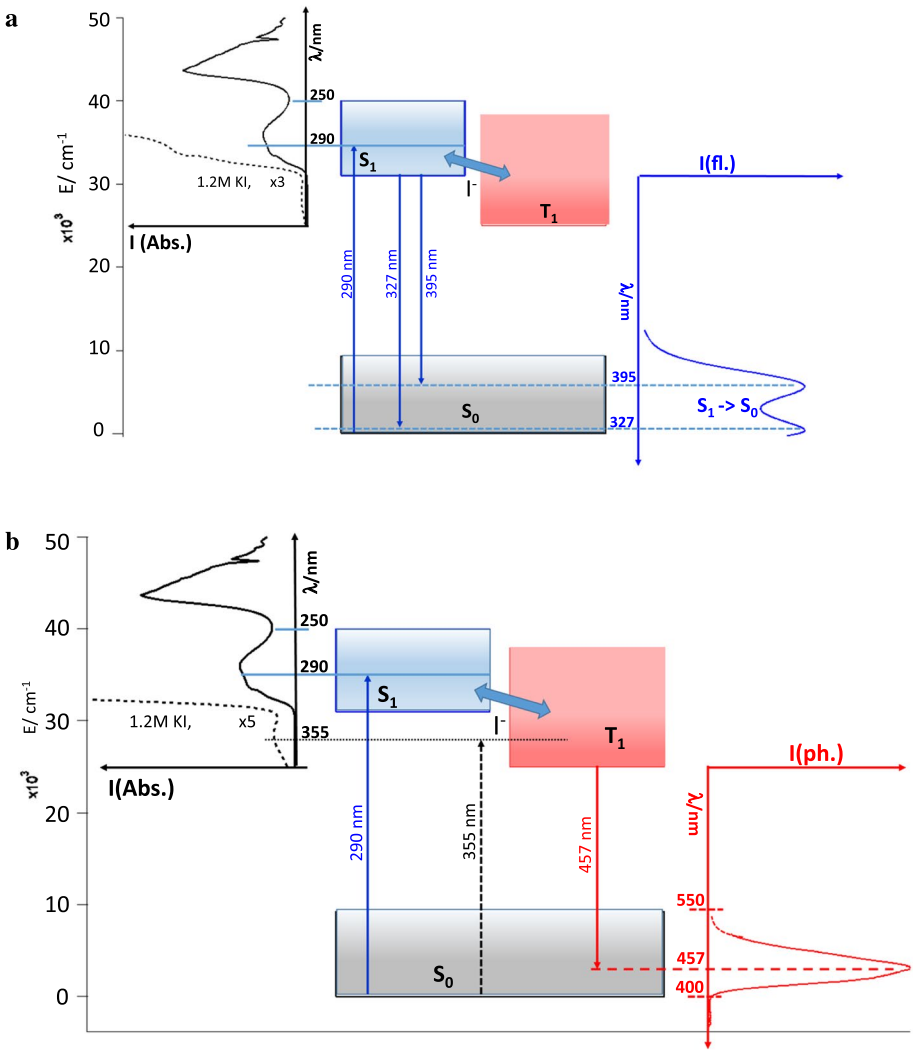

Fig. 2 **a** Energetics of the melatonin system (middle), absorption (left) and fluorescence (right) spectra and relevant $S_1 \leftrightarrow S_0$ transitions (arrows labeled by wavelengths). Detected ranges of the S_0, S_1 and T_1 states are shown as gray-, blue- and red-shaded areas, respectively. Absorption (Abs.) spectra (with (dotted black curve; expanded by × 3) and without (solid black curve) KI) are rotated by 90 degrees to the left. Fluorescence (fl.) spectrum (without KI) is rotated by 90 degrees to the right. Spectra are positioned to match relevant transitions on the energy/wavenumber scale. Transitions relevant to spectral absorption (290 nm) and fluorescence (327 and 395 nm) peaks are shown. Effect of I^- on $S_1 \leftrightarrow T_1$ state mixing is indicated. **b** Energetics of the melatonin system (middle), absorption (left) and phosphorescence (right) spectra and relevant $S_1 \leftarrow S_0$ and $T_1 \leftrightarrow S_0$ transitions (arrows labeled by wavelengths). Detected ranges of the S_0, S_1 and T_1 states are shown as gray-, blue- and red-shaded areas, respectively. Absorption (Abs.) spectra (with (dotted black curve; expanded by × 5) and without (solid black curve) KI) are rotated by 90 degrees to the left. Phosphorescence (ph.) spectrum (with KI) is rotated by 90 degrees to the right. Spectra are positioned to match relevant transitions on the energy/wavenumber scale. Transitions relevant to spectral absorption (290 and 355 nm) and phosphorescence (457 nm) peaks are shown. Effect of I^- on $S_1 \leftrightarrow T_1$ state mixing is indicated

Quenching by halomethanes

Figure 3 shows examples of data relevant to quenching of the melatonin triplet state (T_1) by halomethanes (RX). Figure 3a shows time-resolved phosphorescence data of melatonin without any halomethane quenchers (290 nm excitation; 457 nm, 8 nm resolution luminescence), and Fig. 3b shows Stern–Volmer plots for selected halomethane quenchers. More processed data are to be found in the supporting material. Analyses of the phosphorescence data were based on the assumption that the melatonin triplet state (Me*(T_1)) decay can be separated into three major channels (see (1a–1c) below). (1a): melatonin molecular luminescence, (1b): quenching by chemical components in the solution, other than the halomethanes (Q_0). These could involve processes such as self-quenching and possibly a minor quenching by reactive oxygen species (ROS) according to type I and II mechanisms (Di Mascio et al. 2019) and (1c): quenching by the halomethanes (Q_{RX}),

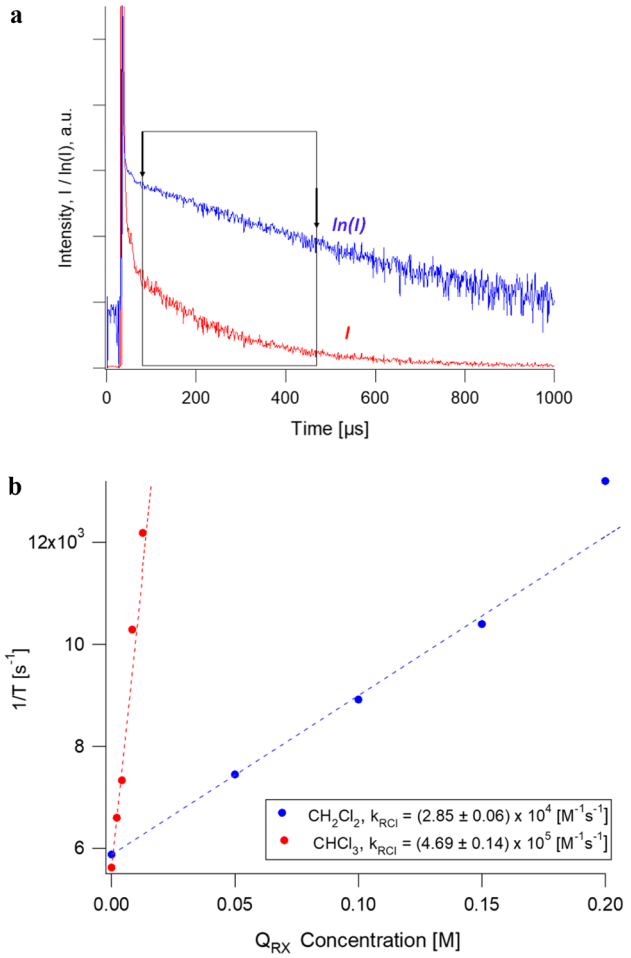

Fig. 3 **a** (i) Time-Correlated Single-Photon Counting (TCSPC) decay curve for melatonin in a solution of Tris pH 8.8 (0.5 M) with potassium iodide (1.2 M) as a HAE inducer and sodium sulfite (2.0×10^{-3} M) as an oxygen scavenger (red) and its logarithmic transformation (blue). The data points in the range marked by the box/arrows of relatively high intensity and linear decrease in ln(*I*) versus *t* were applied for the lifetime evaluation (see main text). **b** Combined Stern–Volmer (SV) plots of melatonin (6.50×10^{-7} M) versus CH_2Cl_2 and $CHCl_3$ concentration, respectively. Solution was buffered in Tris (0.5 M, pH 8.8) with potassium iodide (1.2 M) as a HAE inducer and sodium sulfite (2.0×10^{-3} M) as an oxygen scavenger

$$Me^*(T_1) \xrightarrow{1/\tau_0} Me(S_0) + h\upsilon \tag{1a}$$

$$Me^*(T_1) + Q_0 \xrightarrow{k_0} Me(S_0) + Q_0^* \tag{1b}$$

$$Me^*(T_1) + Q_{RX} \xrightarrow{k_{RX}} Me(S_0) + Q_{RX}^* \tag{1c}$$

where τ_0 is the lifetime of pure melatonin. k_0 and k_{RX} are the quenching rate constants for the Q_0 and Q_{RX}, quenchers, respectively. Energetic assumptions based on the ionization energy of melatonin and electron affinities of the quenchers allowed exclusion of electron transfer processes

Table 1 Quenching rate constants (k_{RX} [M^{-1} s^{-1}]) for quenching of the melatonin triplet state (Me*(T_1)) in association with I^- (I^-···Me*(T_1)) in water

Compounds/quenchers	X = Cl	X = Br
CH_2X_2	$(2.85\pm0.08)\times10^4$	$(2.22\pm0.08)\times10^7$
CHX_3	$(4.19\pm0.16)\times10^5$	$(3.36\pm0.09)\times10^9$
CX_4	$(2.57\pm0.06)\times10^8$	–

(Nist Chemistry webbook, Kuijt et al. 2003). This gives the relationship,

$$\frac{1}{\tau} = \frac{1}{\tau_{eff}} + k_{RX}[Q_{RX}] \tag{2a}$$

where τ is the lifetime of Me*(T_1) in the solution of concern and τ_{eff} is the effective lifetime of Me* (T_1) in the solution (Q_0), without the halomethanes,

$$\frac{1}{\tau_{eff}} = \frac{1}{\tau_0} + k_{RX}[Q_{RX}] \tag{2b}$$

Equation (2a) forms the basis of the Stern–Volmer plots which allow k_{RX} and τ_{eff} to be determined from the slope and intersect values, respectively, of straight line fits of $1/\tau$ as a function of $[Q_{RX}]$. The lifetime (τ) can be determined from the basic relationship between the single-photon counts ($[h\upsilon] = I$/intensity) at time t and τ,

$$\frac{d[h\upsilon]}{dt} \propto -\left(\frac{1}{\tau}\right)[h\upsilon] \tag{3}$$

to give

$$I = I_0 \exp\left(-\left(1/\tau\right)t\right); \tag{4a}$$

$$\ln(I) = -\left(1/\tau\right)t + \ln\left(I_0\right) \tag{4b}$$

where I_0 is the intensity which corresponds to some initial time, $t = 0$. This allows determination of τ from a slope of a plot of ln(I) versus t. Data points for regions of clear single exponential decays were carefully selected for the lifetime evaluations to avoid effects of possible experimental artifacts or unfavorable processes (see Fig. 3a).

The effective lifetime of Me*(T_1) in the solution of concern (Q_0), τ_{eff}, without halomethane quenchers was found to be 197 ± 28 µs. Quenching rate constants, k_{RX}, for CH_xCl_{4-x}; x = 0,1,2 and CH_xBr_{4-x}; x = 1,2 are listed in Table 1 (see also supporting material). Characteristically the quenching rate constants are found to increase by orders of magnitudes with a) number of halogen atoms ($CH_2X_2 < CHX_3 < CX_4$) and b) increasing size of the halogen atoms (Cl < Br).

Possible effect of halomethanes on phosphorescence formation (hence Me*(T_1) formation) was explored by recording luminescence in the phosphorescence spectral region as well as by lifetime measurements. This was performed for solutions with components (Tris buffer (0.5 M, pH 8.8) and sodium sulfite (2.0×10^{-3} M)) other than KI and for the maximum concentration of halomethanes applied in the quenching studies mentioned above. No phosphorescence spectra were detected in the region and any weak background emission detected was found to be from a short lived origin. We therefore concluded that the quenching mechanism for the halomethanes differs from that of the KI/I^-.

Discussion

Phosphorescence

Our data show clear indication of transitions from the lowest energy singlet state (S_1) to the lowest energy triplet state (T_1) as an effect of state mixing, due to spin–orbit coupling induced by the external heavy atom effect (HAE) of I^-. Thus, I^- acts as an efficient quencher for the S_1 state by enhancing an intersystem crossing (isc). Furthermore, the state mixing results in an increased singlet character of the T_1 state but an increased triplet character of the S_1 state, former of which shows as an enhanced transition probability for the $T_1 \leftarrow S_0$ photon transition. Thus, I^- also acts as a quencher for the T_1 state by enhancing the transition probability for the $T_1 \rightarrow S_0$ transition. Similarly, although not as clear from the data (due to spectra overlap; see Fig. 1a), a diminished transition probability for the $S_1 \leftrightarrow S_0$ transitions is to be expected. While the quenching effects of I^- will mainly be in the form of an alteration in transition probabilities (both isc and emission), quenching by means of electron energy transfer should be negligible, since an energy exchange from Me*(T_1) to I^- will involve an improbable nonresonant excitation of I^- to form $I + e^-$ rather than a resonant process.

Quenching

While the quenching by I^- is primarily due to HAE, as mentioned above, the data relevant to quenching by the halomethanes, which differs dramatically from that for I^- (see above), suggest that it is different in nature. We conclude that it primarily involves electron energy transfer, based on the following arguments ((i)–(iii)),

i. Absorption spectra of the halomethane quenchers used allowed an estimate of the lower energy limits for their lowest energy excited singlet states ($S_1(Q,$ min)) which are accessible by photon absorption (Keller-Rudek et al. 2013). This is presented in Fig. 4

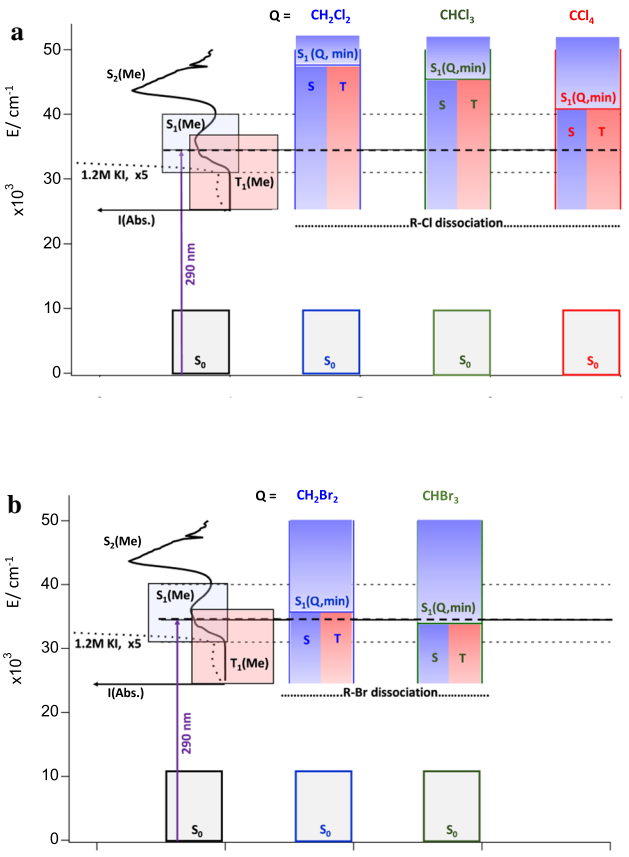

Fig. 4 Semi-schematic energy diagrams relevant to quenching of the excited melatonin (Me*(T_1, S_1)) in the presence of I^- by the halomethanes CH_2Cl_2, $CHCl_3$ and CCl_4 (**a**) and CH_2Br_2 and $CHBr_3$ (**b**). Lower limits of the lowest excited singlet states of the quenchers accessible by photon absorption are marked by S_1(Q,min). Variation in number and density of triplet (T) and singlet (S) states within Q_{RX} below S_1(Q,min) is indicated by color gradients (blue for S and red for T). Absorption (Abs.) spectra (with (dotted black curve; expanded by ×5) and without (solid black curve) KI) are rotated by 90 degrees to the left. Observed limits for the S_1 and T_1 states of melatonin are indicated by boxes. S_0 are the corresponding ground states. Transition relevant to the excitation (290 nm) is shown

along with absorption spectra for melatonin. The figure shows that these energy limits ($S_1(Q,$ min)) are either higher than or approximately the same as the photoexcitation (290 nm) energy and shifts in energy as $CH_2X_2 > CHX_3 > CX_4$ and Cl > Br. Hidden (non-accessible by photon excitation) triplet states will be in the same energy region and lower in energy. It is a reason to believe that the energies for photodissociative states (both triplet (T) and singlet (S) states) accessible for energy transfer upon collision with Me*(T_1) (created by photoexcitation) will follow the same energy trend (i.e., $CH_2X_2 > CHX_3 > CX_4$ and Cl > Br). Furthermore, the number of states will increase with the number of halogen atoms in the molecules (i.e., as $CH_2X_2 < CHX_3 < CX_4$). Therefore, the

probability of energy transfer to lower energy excited T and S states within the quenchers will vary as $CH_2X_2 < CHX_3 < CX_4$ and Cl < Br. This closely correlates with the trends in the quenching rates constants (i.e., $CH_2X_2 < CHX_3 < CX_4$ and Cl < Br; see earlier), which strongly suggests that the quenching primarily occurs via electron energy transfer.

ii. The quenching rate constants for the halomethane quenchers vary in order of magnitude both with the number and size of the halogen atoms (k_{RX}; Table 1). This is what to expect if the rate constants are exponentially dependent on the governing factor. Single-step second-order rate constants are primarily determined by the collision frequencies ($Z_{Me,Q}$), steric factors (P) and activation energies (E_a). Of these terms, the rate constant is exponentially dependent on the last term (E_a) only. In a collision between the quenchers (Q_{RX}) and the Me*(T_1) complex to form Me(S_0) and *T/S* excited states of the quenchers $Q^*_{RX}(T,S)$, the activation energy will depend on the potential energy of a potential energy surface in the energy transfer process. Judging from the argument in (i) above and Fig. 4**,** there is a reason to believe that E_a will vary with Q_{RX} as $CH_2X_2 > CHX_3 > CX_4$ and Cl > Br to give rate constants exponentially depending on Q_{RX} as $CH_2X_2 < CHX_3 < CX_4$ and Cl < Br.

iii. It has been shown that the change in the phosphorescence rate constant of aromatic hydrocarbons due to heavy atom effects falls of rapidly (exponentially) with the distance of the heavy atom to the photoactive side of the chromophore (Najbar et al. 1978). Quenching and coupling effects of the Q_{RX} might be expected to increase with the number of halogen atoms in the RX compound as $CH_2X_2 < CHX_3 < CX_4$ if heavy atom effects were the reason. However, one would not expect a dramatic difference in such effects with the number of halogen atoms (whether 2,3 or 4) in the quenching molecule since the halogen atom(s) closest to the photoactive side will be most effective, whereas the effect of those atoms further away, for steric reasons, will be much less. This is in contrast with our observation of a dramatic/exponentially dependent difference in the rate constants with the number of halogen atoms ($CH_2X_2 < CHX_3 < CX_4$) suggesting that a HAE is not a major factor.

Absorption spectra (Causley and Russell 1975; Eden et al. 2007; Keller-Rudek et al. 2013), photofragmentation studies (Van Veen et al. 1985; Blanchet et al. 2009; Hafliðason et al. 2018, 2019) and/or potential energy calculations (Ajitha et al. 2004; Escure et al. 2009; Granucci et al. 2010) for chlorine- and bromine-containing halomethane molecules reveal the nature of excited electronic states in the energy range within the photoexcitation used here (290 nm) and lower limits of the S_1 and T_1 states of melatonin as detected here (see Fig. 4a, b). These excited states might serve as the donors in the proposed electron energy transfer of concern. For all the halomethanes use here, the excited states within this energy range both T and S state correspond to excitations of electrons from nonbonding orbitals (n) localized on the halogen atoms to antibonding (σ^*) molecular orbitals to result in repulsive potential energy curves for the C–X bonds and therefore a corresponding dissociation. The lowest energy bound excited states, which correspond to excitations of the nonbonding halogen atom orbitals (n) to high-energy Rydberg electron molecular orbitals, are much higher in energy (Escure et al. 2009; Keller-Rudek et al. 2013). Furthermore, the dissociation energies of the molecules to form R and X are lower in energy than the energy range of concern (Nist Chemistry webbook). Therefore, most probably, electron energy transfer from the melatonin complex to the halomethane molecules will result in dissociation of R–X bonds to form R and X fragments.

Lifetime (τ_{eff})

The triplet state lifetime of melatonin has been less documented than those of related molecules like tryptophan or its precursor, indole. Our effective lifetime of melatonin ($\tau_{eff} = 197 \pm 28$ µs) reported here refers to the lifetime of the $I^- \cdots Me^*(T_1)$ complex in the water solution of concern (Tris pH 8.8 buffer, sodium sulfite (2.0×10^{-3} M) and potassium iodide (1.2 M); see above) at an ambient temperature not defined precisely. This lifetime is of the same order of magnitude, but longer than the approximate value of 107 µs at 20 ± 1 °C reported by Amjadi et al. for similar solutions (Amjadi et al. 2006). When our value is compared to the well documented but disagreed upon indole in water at 20 °C, it is considerably lower than values reported by Strambini et al. (Strambini and Gonnelli 1995; Strambini et al. 2004). Later reported value by Kowalska-Baron et al. of 110 µs for indole in water at 20 °C is of the same order of magnitude and closer to our value, although lower (Kowalska-Baron et al. 2012). In 2013, Kowalska-Baron et al. reported the triplet state lifetime of indole carboxylated in positions 2 and 5 in water at 20 °C as 912 and 56 µs, respectively (Kowalska-Baron et al. 2013). It is noticeable that our value for melatonin, which also has functional groups, albeit different, in the same positions, is within that range. It should be emphasized, however, that the influence of the surroundings on the lifetime cannot be ignored in this context, since all solubilized molecules contribute to a quenching to affect the effective lifetime ($\tau_{eff;}$ see Eq. (2a, 2b)) and molecular movement governed by temperature can influence quenching dramatically (Amjadi et al. 2006). In addition, self-quenching and

triplet–triplet annihilation could also be involved to some extent (Strambini et al. 2004).

Summary and conclusions

Absorption, fluorescence and phosphorescence spectra were recorded for melatonin in solutions of Tris buffer (0.5 M, pH 8.8) and 1.7×10^{-4} M melatonin for the absorption spectra and of Tris buffer (0.5 M, pH 8.8), sodium sulfite (2×10^{-3} M) and 6.5×10^{-7} M melatonin for the luminescence spectra as a function of KI concentrations (Fig. 1). The absorption spectra structure in the region of 200–400 nm (Fig. 1a) is indicative of transitions from the singlet ground state (S_0) to excited singlet states S_1 ($\lambda < 250$ nm), S_n ($n > 1$) as well as to the first excited triplet state T_1. The spectra due to the $S_n \leftarrow S_0$ transitions are found to build up gradually with KI concentration in the region of about 230–275 nm, and a weak absorption due to the forbidden $T_1 \leftarrow S_0$ transition appears and increases in intensity in the region of 325–400 nm (with a peak at 355 nm) as KI is added. Fluorescence spectra created by 290 nm excitation in the 320–540 nm region (Fig. 1b) due to the $S_1 \rightarrow S_0$ transition are found to decrease in intensity as the KI concentration increases. While no phosphorescence is observed in solutions without KI for 290 nm excitation, phosphorescence spectra in the region of 400–550 nm (Fig. 1c) appear and grow gradually as KI is added. A close correlation is found between the decrease in the fluorescence and the increase in the phosphorescence. These observations allow an estimate of energy ranges and limits for the S_0, S_1 and T_1 states of relevance to the absorption and luminescence processes (Fig. 2). Furthermore, the structure and intensity alterations with KI concentration are attributed to an external heavy atom effect of I^- on melatonin in a $I^- \cdots$Me complex, which causes mixing of the S_1 and T_1 states due to an induced spin–orbit coupling. This causes enhancement in intersystem crossing from S_1 to T_1 as well as alterations in the emission transitions to decrease and increase the $S_1 \rightarrow S_0$ and $T_1 \rightarrow S_0$ transition probabilities, respectively. Time-Correlated Single-Photon Counting (TCSPC) decay curves for the phosphorescence at 457 nm (8 nm resolution) after 290 nm excitation were recorded for melatonin in solutions of Tris pH 8.8 buffer, sodium sulfite (2.0×10^{-3} M) and potassium iodide (1.2 M) as a function of the halomethane (RX) quenchers CH_2Cl_2, $CHCl_3$, CCl_4, CH_2Br_2 and $CHBr_3$ concentrations. The $I^- \cdots Me^*(T_1)$ complex phosphorescence lifetimes were determined from the curves to give quenching rate constants (k_{RX}) from Stern–Volmer plots. The effective lifetime (τ_{eff}) of the complex in a solution without any halomethane quenchers was determined to be 197 ± 28 µs. Dramatic (exponentially dependent) alteration was observed in the rate constants depending on the quenchers, varying as $CH_2X_2 < CHX_3 < CX_4$ and Cl < Br (see Table 1). These quenching effects are attributed to energy transfer from $I^- \cdots Me^*(T_1)$ to low-lying electronic (triplet and/or singlet) states of the halomethanes followed by dissociation to form the R and X fragments.

The usefulness of photosensitizers is diverse. Thus, e.g., photosensitizers can be used as probes for structural determination of its surrounding based on changes in its luminescence properties and photosensitizers have been proposed as important components in light-sensitive intelligent drug delivery systems for releasing active molecules at appropriates sites (Alvarez-Lorenzo et al. 2009; Salem et al. 2019). Its use in organic media like gels or inside cavities such as micelles, liposomes or nanocomposites is of particular importance. We feel that the data and results presented here adds to information and understanding relevant to important properties as well as effects of photosensitizers and/or as probes in organic media. First, the effect of a heavy atom (external or internal HAE) in close vicinity of the photoactive site of the sensitizing molecule can be of great importance to increase the lifetime of the sensitizer by inducing an intersystem crossing from a singlet state to a triplet state by an effective state mixing. Second, an electron energy transfer can occur very rapidly from a donor/sensitizer to an acceptor molecule in cases where accessible low-energy excited (triplet or singlet) electronic states are accessible (i.e., lower in energy than the donor/sensitizer excited state(s)). Third, low-energy excited states of acceptor molecules frequently correspond to repulsive states (corresponding to a transfer of electrons from bonding to antibonding orbitals) in nature which can lead to bond dissociation (single bonds) or distortions (i.e., double bonds). Although the systems studied and presented in this paper deals with interaction of an organic sensitizer with halogen containing reagents as presented and summarized schematically in Fig. 5a**,** it could have an important analogy to interactions of a sensitizer with organic compounds as demonstrated in Fig. 5b. The energies of electronic states of conjugated or aromatic organic molecules corresponding to excitation of π electrons to π^* typically are relatively low (depending on the size of the conjugated/aromatic molecular system). An effect of such an excitation of a molecule by an energy transfer from a sensitizer effectively breaks the double bond partly (i.e., disrupts the π bond component of the double bond) which allows free rotation around the bond followed by possible conformational changes.

We hope that this work will prompt further theoretical as well as experimental investigations which might aid in clarifying the nature and interpretations proposed here. Thus, for example, whereas bond braking of the halomethanes as an effect of energy transfer is proposed and highly probable, both potential energy surface calculations and experimental

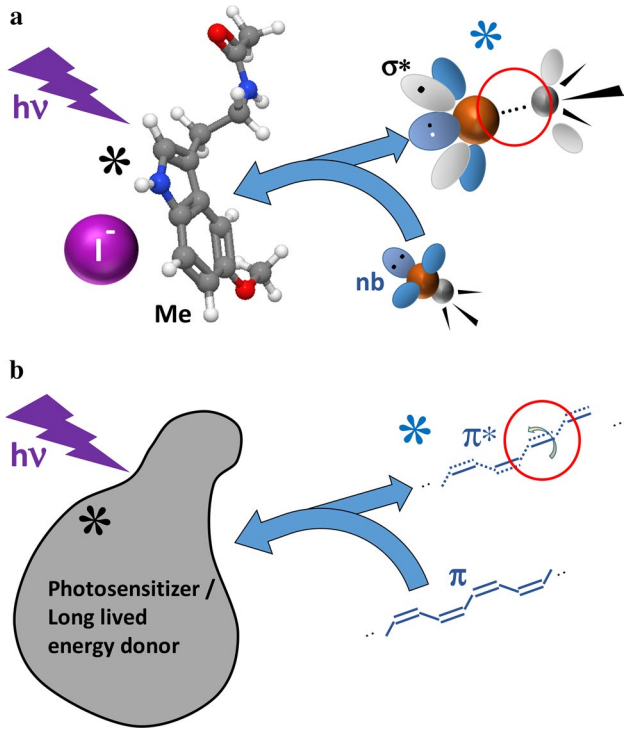

Fig. 5 **a** Schematic figure demonstrating the nature of the melatonin sensitizer with respect to structure ($I^{-}\cdots Me$), photon excitation (hν), collision with a halomethane molecule (R-X), excitation by energy transfer and $R^{\cdots}X$ dissociation (red circle). **b** Schematic figure demonstrating the nature of a long-lived sensitizer in terms of photon excitation (hν), collision with a conjugated molecular system, excitation by energy transfer and partial bond rupture/conformational changes (red circle/arrow)

evidence would be valuable and the phosphorescence lifetime for melatonin needs clarification to name but few.

Supplementary Information The online version contains supplementary material available at https://doi.org/10.1007/s11696-022-02222-z.

Acknowledgements The financial support of Rannís and the Technological Developments Fund (Grant No. 186857-0611) and the University Research Fund, University of Iceland, is gratefully acknowledged.

Declarations

Conflict of interest There are no conflicts to declare.

Open Access This article is licensed under a Creative Commons Attribution 4.0 International License, which permits use, sharing, adaptation, distribution and reproduction in any medium or format, as long as you give appropriate credit to the original author(s) and the source, provide a link to the Creative Commons licence, and indicate if changes were made. The images or other third party material in this article are included in the article's Creative Commons licence, unless indicated otherwise in a credit line to the material. If material is not included in the article's Creative Commons licence and your intended use is not permitted by statutory regulation or exceeds the permitted use, you will need to obtain permission directly from the copyright holder. To view a copy of this licence, visit http://creativecommons.org/licenses/by/4.0/.

References

Aaron JJ, Fisher R, Winefordner JD (1974) Analytical study of the phosphorescence of pyrimidine derivatives in frozen aqueous solution. Talanta 21(11):1129–1135. https://doi.org/10.1016/0039-9140(74)80096-2

Ajitha D, Wierzbowska M, Lindh R, Malmqvist PA (2004) Spin-orbit ab initio study of alkyl halide dissociation via electronic curve crossing. J Chem Phys 121(12):5761–5766. https://doi.org/10.1063/1.1784411

Alvarez-Lorenzo C, Bromberg L, Concheiro A (2009) Light-sensitive intelligent drug delivery systems. Photochem Photobiol 85(4):848–860. https://doi.org/10.1111/j.1751-1097.2008.00530.x

Amjadi M, Manzoori JL, Miller JN (2006) Study of the heavy atom-induced room temperature phosphorescence properties of melatonin and its analytical application. Spectrochim Acta Part A Mol Biomol Spectrosc 63(2):337–342. https://doi.org/10.1016/j.saa.2005.05.019

Bent DV, Hayon E (1975) Excited state chemistry of aromatic amino acids and related peptides III Tryptophan. J Am Chem Soc 97(10):2612–2619. https://doi.org/10.1021/ja00843a004

Blanchet V, Samartzis PC, Wodtke AM (2009) UV photodissociation of methyl bromide and methyl bromide cation studied by velocity map imaging. J chem phys 130(3):034304. https://doi.org/10.1063/1.3058730

Bolmatov D, McClintic WT, Taylor G, Stanley CB, Do C, Collier CP, Leonenko Z, Lavrentovich MO, Katsaras J (2019) Deciphering melatonin-stabilized phase separation in phospholipid bilayers. Langmuir 35(37):12236–12245. https://doi.org/10.1021/acs.langmuir.9b01534

Braslavsky S, Houk KN (2003) Glossary of terms used in photochemistry. Pure Appl Chem 60:1055–1106. https://doi.org/10.1016/B978-044451322-9/50034-8

Causley GC, Russell BR (1975) Vacuum ultraviolet absorption spectra of the bromomethanes. J Chem Phys 62(3):848–857. https://doi.org/10.1063/1.430535

de Lima VR, Caro MS, Munford ML, Desbat B, Dufourc E, Pasa AA, Creczynski-Pasa TB (2010) Influence of melatonin on the order of phosphatidylcholine-based membranes. J Pineal Res 49(2):169–175. https://doi.org/10.1111/j.1600-079X.2010.00782.x

Di Mascio P, Martinez GR, Miyamoto S, Ronsein GE, Medeiros MHG, Cadet J (2019) Singlet molecular oxygen reactions with nucleic acids, lipids, and proteins. Chem Rev. https://doi.org/10.1021/acs.chemrev.8b00554

Drolle E, Kučerka N, Hoopes MI, Choi Y, Katsaras J, Karttunen M, Leonenko Z (2013) Effect of melatonin and cholesterol on the structure of DOPC and DPPC membranes. Biochim et Biophys Acta (BBA)-Biomembr 1828 9:2247–2254. https://doi.org/10.1016/j.bbamem.2013.05.015

Easley CJ, Mettry M, Moses EM, Hooley RJ, Bardeen CJ (2018) Boosting the heavy atom effect by cavitand encapsulation: room temperature phosphorescence of pyrene in the presence of oxygen. J Phys Chem A 122(32):6578–6584. https://doi.org/10.1021/acs.jpca.8b05813

Eden S, Limão-Vieira P, Hoffmann SV, Mason NJ (2007) VUV spectroscopy of CH3Cl and CH3I. Chem Phys 331(2):232–244. https://doi.org/10.1016/j.chemphys.2006.10.021

Egorov SY, Krasnovsky AA Jr, Bashtanov MY, Mironov EA, Ludnikova TA, Kritsky MS (1999) Photosensitization of singlet oxygen formation by pterins and flavins. Biochem (Mosc) 64(10):1117–1121

Escure C, Leininger T, Lepetit B (2009) Ab initio study of valence and Rydberg states of CH3Br. J Chem Phys 130:244306. https://doi.org/10.1063/1.3152865

Fischer CJ, Gafni A, Steel DG, Schauerte JA (2002) The triplet-state lifetime of indole in aqueous and viscous environments: significance to the interpretation of room temperature phosphorescence in proteins. J Am Chem Soc 124(35):10359–10366. https://doi.org/10.1021/ja016609x

Gershenson A, Schauerte JA, Giver L, Arnold FH (2000) Tryptophan phosphorescence study of enzyme flexibility and unfolding in laboratory-evolved thermostable esterases. Biochem 39(16):4658–4665. https://doi.org/10.1021/bi992473s

Giachino GG, Kearns DR (1970) Nature of the external heavy-atom effect on radiative and nonradiative singlet-triplet transitions. J Chem Phys 52(6):2964–2974. https://doi.org/10.1063/1.1673425

Goswami S, Haldar C (2015) Melatonin as a possible antidote to UV radiation induced cutaneous damages and immune-suppression: an overview. J Photochem Photobiol B 153:281–288. https://doi.org/10.1016/j.jphotobiol.2015.10.006

Granucci G, Medders G, Velasco A (2010) Potential energy surfaces of the first three singlet states of CH3Cl. Chem Phys 500:202–206. https://doi.org/10.1016/j.cplett.2010.10.011

Hafliðason A, Glodic P, Koumarianou G, Samartzis PC, Kvaran Á (2018) Multiphoton Rydberg and valence dynamics of CH3Br probed by mass spectrometry and slice imaging. Phys Chem Chem Phys 20(25):17423–17433. https://doi.org/10.1039/C8CP02350F

Hafliðason A, Glodic P, Koumarianou G, Samartzis PC, Kvaran Á (2019) Two-color studies of CH3Br excitation dynamics with MPI and slice imaging. Phys Chem Chem Phys 21(20):10391–10401. https://doi.org/10.1039/C8CP06376A

Imakubo K (1985) Intrinsic emission properties of trinucleotides at 293 and 77 K. Nucleic Acids Symp Ser 16:17–20

Jayaraj N, Maddipatla M, Prabhakar R, Jockusch S, Turro NJ, Ramamurthy V (2010) Closed nanocontainer enables thioketones to phosphoresce at room temperature in aqueous solution. J Phys Chem B 114(45):14320–14328. https://doi.org/10.1021/jp911698s

Jin CS, Zheng G (2011) Liposomal nanostructures for photosensitizer delivery. Lasers Surg Med 43(7):734–748. https://doi.org/10.1002/lsm.21101

Keller-Rudek H, Moortgat GK, Sander R, Sörensen R (2013) The MPI-mainz UV/VIS spectral atlas of gaseous molecules of atmospheric interest. Earth Syst Sci Data 5(2):365–373. https://doi.org/10.5194/essd-5-365-2013

Kim H, Crouch SR, Zabik MJ, Selim SA (1990) Environmental factors affecting micellar stabilized room-temperature phosphorescence lifetimes. Anal Chem 62(21):2365–2369. https://doi.org/10.1021/ac00220a019

Kotel'nikova RA, Tat'ianenko LV, Mekler VM, Kotel'nikov AI (1982) Study of catalytically active center of the Ca2+-Mg2+-dependent ATPase of sarcoplasmic reticulum by triplet probe method. Mol Biol (mosk) 16(6):1188–1194. https://doi.org/10.1016/S0006-3495(89)82681-5

Kowalska-Baron A, Chan M, Gałęcki K, Wysocki S (2012) Photophysics of indole, tryptophan and N-acetyl-L-tryptophanamide (NATA): heavy atom effect. Spectrochim Acta A Mol Biomol Spectrosc 98:282–289. https://doi.org/10.1016/j.saa.2012.08.017

Kowalska-Baron A, Gałęcki K, Wysocki S (2013) Photophysics of indole-2-carboxylic acid (I2C) and indole-5-carboxylic acid (I5C): Heavy atom effect. Spectrochim Acta Part A Mol Biomol Spectrosc 116:183–195. https://doi.org/10.1016/j.saa.2013.07.011

Kowalska-Baron A, Gałęcki K, Wysocki S (2015) Room temperature phosphorescence study on the structural flexibility of single tryptophan containing proteins. Spectrochim Acta A Mol Biomol Spectrosc 134:380–387. https://doi.org/10.1016/j.saa.2014.06.122

Krasnovsky AA Jr, Belyaeva OB, Kovalev YV, Ignatov NV, Litvin FF (1999) Phosphorescence of intermediates of the terminal stage of chlorophyll biosynthesis in plants. Biochemistry (mosc) 64(5):587–591

Kuijt J, Ariese F, Brinkman UAT, Gooijer C (2003) Room temperature phosphorescence in the liquid state as a tool in analytical chemistry. Anal Chim Acta 488(2):135–171. https://doi.org/10.1016/S0003-2670(03)00675-5

Lajunen T, Nurmi R, Kontturi L, Viitala L, Yliperttula M, Murtomaki L, Urtti A (2016) Light activated liposomes: functionality and prospects in ocular drug delivery. J Control Release 244(Pt B):157–166. https://doi.org/10.1016/j.jconrel.2016.08.024

Lepeshkevich SV, Parkhats MV, Stasheuski AS, Britikov VV, Jarnikova ES, Usanov SA, Dzhagarov BM (2014) Photosensitized singlet oxygen luminescence from the protein matrix of Zn-substituted myoglobin. J Phys Chem A 118(10):1864–1878. https://doi.org/10.1021/jp501615h

Li Z, Galley WC (1989) Evidence for ligand-induced conformational changes in proteins from phosphorescence spectroscopy. Biophys J 56(2):353–360. https://doi.org/10.1016/s0006-3495(89)82681-5

Massiot J, Makky A, Di Meo F, Chapron D, Trouillas P, Rosilio V (2017) Impact of lipid composition and photosensitizer hydrophobicity on the efficiency of light-triggered liposomal release. Phys Chem Chem Phys 19(18):11460–11473. https://doi.org/10.1039/c7cp00983f

Matthíasson K, Koumarianou G, Jiang M-X, Glodic P, Samartzis PC, Kvaran Á (2020) Formation of highly excited iodine atoms from multiphoton excitation of CH3I. Phys Chem Chem Phys 22(9):4984–4992. https://doi.org/10.1039/C9CP06242D

Mersol JV, Steel DG, Gafni A (1993) Detection of intermediate protein conformations by room temperature tryptophan phosphorescence spectroscopy during denaturation of *Escherichia coli* alkaline phosphatase. Biophys Chem 48(2):281–291. https://doi.org/10.1016/0301-4622(93)85015-a

Mersol J, Gershenson A, Steel D, Gafni A (1992) Applications of room-temperature tryptophan phosphorescence to the study of protein structure and dynamics. SPIE Time-Resolved Laser Spectros Biochem III 1640:462–472. https://doi.org/10.1117/12.58238

Minaev B (2004) Theoretical study of the external heavy atom effect on phosphorescence of free-base porphin molecule. Spectrochim Acta A Mol Biomol Spectrosc 60(13):3213–3224. https://doi.org/10.1016/j.saa.2004.03.005

Montes-Navajas P, Garcia H (2010) Cucurbituril Complexation Enhances Intersystem Crossing and Triplet Lifetime of 2,4,6-Triphenylpyrylium Ion. J Phys Chem C 114(5):2034–2038. https://doi.org/10.1021/jp9095166

Najbar J, Rodakiewicz-Nowak J, Chodkowska A (1978) External heavy atom effect on the triplet state of aromatic hydrocarbons: IV. Fluorene, triphenylene-d12 and coronene. J Lumin 17(4):449–465. https://doi.org/10.1016/0022-2313(78)90054-6

Nist Chemistry webbook. National Institute of Standards and Technology. https://webbook.nist.gov/chemistry/nameser/

Qin Y, Chen LJ, Dong F, Jiang ST, Yin GQ, Li X, Tian Y, Yang HB (2019) Light-controlled generation of singlet oxygen within a discrete dual-stage metallacycle for cancer therapy. J Am Chem Soc. https://doi.org/10.1021/jacs.9b02726

Rath MC, Mahal HS, Mukherjee T (1999) Photophysics of melatonin in different environments. Photochem Photobiol 69(3):294–300. https://doi.org/10.1562/0031-8655(1999)069%3c0294:pomide%3e2.3.co;2

Reiter RJ, Tan D-X, Galano A (2014) Melatonin reduces lipid peroxidation and membrane viscosity. Front Physiol 5:377–377. https://doi.org/10.3389/fphys.2014.00377

Salem JK, El-Nahhal IM, Salama SF (2019) Determination of the critical micelle concentration by absorbance and fluorescence techniques using fluorescein probe. Chem Phys Lett 730:445–450. https://doi.org/10.1016/j.cplett.2019.06.038

Strambini GB, Gonnelli M (1995) Tryptophan Phosphorescence in Fluid Solution. J Am Chem Soc 117(29):7646–7651. https://doi.org/10.1021/ja00134a008

Strambini GB, Kerwin BA, Mason BD, Gonnelli M (2004) The Triplet-state Lifetime of Indole Derivatives in Aqueous Solution. Photochem photobiol 80(3):462–470. https://doi.org/10.1111/j.1751-1097.2004.tb00115.x

Van Veen GNA, Baller T, De Vries AE (1985) Photofragmentation of CH3Br in the A band. Chem Phys 92(1):59–65. https://doi.org/10.1016/0301-0104(85)80005-7

White W, Seybold PG (1977) External heavy-atom effect on the room-temperature luminescence of adsorbed dyes. J Phys Chem 81(21):2035–2040. https://doi.org/10.1021/j100536a017

Zhang D, Gong C, Wang J, Xing D, Zhao L, Li D, Zhang X (2021) Unravelling melatonin's varied antioxidizing protection of membrane lipids determined by its spatial distribution. J Phys Chem Lett 12(31):7387–7393. https://doi.org/10.1021/acs.jpclett.1c01965

Publisher's Note Springer Nature remains neutral with regard to jurisdictional claims in published maps and institutional affiliations.